Journal of Inflammation Research

Dovepress
open access to scientific and medical research

Open Access Full Text Article

ORIGINAL RESEARCH

Structural Modeling of Wild and Mutant Forms of Human Plasma Platelet Activating Factor-Acetyl Hydrolase Enzyme

This article was published in the following Dove Press journal:
Journal of Inflammation Research

Mohd Imran Khan
Gururao Hariprasad

Department of Biophysics, All India Institute of Medical Sciences, New Delhi 110029, India

Purpose: To investigate the structural features of wild and mutant forms of the pPAF-AH enzyme that are responsible for coronary artery disease.

Methods: Mutant variants of human pPAF-AH having either V279F, Q281R, or both were modelled and evaluated for stereo chemical and structural correctness. The 3D coordinates of substrate PAF were retrieved from the PubChem database was solvated and minimized on Discovery Studio, and docked to the wild and mutant enzyme models. The top docked pose complex was refined by MD simulation.

Results: pPAF-AH model comprises of 420 amino acids in a α/β-hydrolase fold that contains a substrate-binding hydrophobic channel with an active site pocket having a catalytic triad of Ser273, Asp296 and His351. Mutations at positions 279 and 281 are opposite one another on the middle of 12 residues long H5 helix that forms the hydrophobic core of the enzyme. V279F causes a tilt on the axis of the mutation bearing helix to avoid steric clashes with the hydrophobic residues on the β-sheets adjacent to it, inducing subtle conformational changes on the H5-β8 loop, β8 sheet, and the loop bearing Asp296. A cascade of conformational changes induces a change in the orientation of His351 resulting in loss of hydrogen bonded interaction with catalytic Ser273. Q281R causes a shortening of H5 and β8, which induces conformational changes of the loops bearing Ser273 and Asp296, respectively. Simultaneous conformational changes of secondary structural elements result in the flipping of His351 causing a break in the catalytic triad. Also, there is a compromise in the substrate-binding area and volume in the mutants resulting in loss of binding to its substrate.

Conclusion: Mutant enzymes show changes at the site of the mutation, secondary motif conformations and global structural conformations that adversely affect the active site, decrease substrate channel volume and decrease stability, thereby affecting enzymatic function.

Keywords: platelet activating factor acetyl hydrolase, structure, molecular modelling, mutations, V279F, Q281R, clinical phenotype, coronary artery disease

Introduction

Phospholipases A_2 (PLA_2, EC 3.1.1.4) are acyl esterases that catalyze the hydrolysis of glycerol-phospholipids at the *sn-2* position of the glycerol backbone to release free fatty acids and lysophospholipids.[1] They are upstream regulators of many inflammatory processes.[2] In mammals, PLA_2s play an important role in various biological processes, including homeostasis of cellular membranes, lipid digestion, host defense, and production of potent lipid mediators such as

Correspondence: Gururao Hariprasad
Tel +91-11-26594240
Fax +91-11-26588663
Email g.hariprasad@rediffmail.com

submit your manuscript | www.dovepress.com
DovePress
http://doi.org/10.2147/JIR.S274940

eicosanoids and lysophospholipids, which in turn exert a wide variety of housekeeping functions under physiological conditions and inflammatory functions in certain pathologies.[3–5]

The very first classification for PLA_2 enzymes was based on the sequence, evolutionary origin and pharmacological implications.[6] Subsequently, the PLA_2 superfamily of enzymes was classified based on catalytic function, amino acid composition, and identifiable sequence homology.[4] Recently, the PLA_2were collectively classified into six categories, namely: secreted PLA_2s, cytosolic PLA_2s, calcium independent PLA_2s, adipose-specific PLA_2s, lysosomal PLA_2s, and platelet activating factor acetyl hydrolases (PAF-AH).[7]

PAF-AH is a member of the serine-dependent class of A_2 phospholipases. There are four members in this family of which three are intracellularly expressed (PAF-AHs), and the fourth member is secreted extracellularly and is found in the plasma in circulation (pPAF-AH).[8] pPAF-AH is located at 6p12-p21.1, has a molecular weight of 45 kDa encoding 441 amino acids protein. The enzyme acts on phospholipids from the surface of cell membranes, native lipoproteins and oxidatively-modified lipoproteins to generate downstream multiple bioactive lipid products that includes lyso-platelet acting factor (Lyso-PAF), and oxidized non-esterified fatty acids (Ox-NEFA) with certain biological properties and functions.[9–11] pPAF-AH is found associated with LDL and HDL in human plasma, and is therefore also known as Lp-PLA_2.[12] The enzyme pPAF-AH hydrolyzes the ester bond at the *sn-2* position of platelet activating factor (PAF), resulting in its degradation and inactivation.[13] Apart from PAF, it also degrades other structurally related oxidized phospholipids that have an oxidatively modified fatty acyl chain at the *sn-2* position. The enzymatic catalysis is by the virtue of the classical lipase α/β-serine hydrolase fold comprising of a catalytic triad consisting of serine, aspartate and histidine.[14,15]

Plasma pPAF-AH degrades not only PAF but also oxidatively fragmented phospholipids with potent biological activities. This is a reason pPAF-AH and their mutations have implications in certain clinical conditions such as asthma, sepsis, Hemolytic Uremic syndrome and cardio vascular diseases.[16,17] The products of two separate enzymatic reactions that involve substrates PAF and short chain *sn-2* moieties such as phosphatidylcholine results in lyso-PAF and lyso-phosphatidylcholine.[18,19] These products of two separate enzymatic reactions have varying effects on plaque formation in coronary arteries, wherein they lead to pro-atherosclerotic and anti-atherosclerotic clinical phenotypic outcomes.[20,21] In accordance, the mutations such as V279F and Q281R on pPAF-AH too have been known to have critical and favorable cardiovascular outcomes.[22–25]

Structural characterization of the PLA_2 group of enzymes has helped: (1) to understand the structure-function relationship of PLA_2 enzymes;[26] (2) to sub-classify the groups and sub-groups within the PLA_2 family;[27] (3) to understand the mechanism of PLA_2 induced toxicity;[28] (4) to delineate the structural elements of druggable PLA_2s for potent drug design;[28,29] (6) to pave the way for personalised medicine in PLA_2 mediated diseases;[30] (7) to understand the effect of mutations on PLA_2enzyme function and thereby their impact on clinical phenotypes.[31]

In this study, we have carried out modeling studies of wild and mutant forms of pPAF-AH to understand the implications of mutations V279F, Q281R, V279F +Q281R on their respective structures. The understanding of which is important to comprehend the pathogenesis of disease, thereby laying the platform for the development of appropriate therapeutic interventions.

Methods

Sequence Analysis

Protein sequences of pPAF-AH from human (Q13093), pig (Q4Z8N7), mouse (Q60963), rabbit (G1SE06) and sheep (W5PMY0) were retrieved from the National Centre for Biotechnology Information.[32] Sequences were aligned using Clustal Omega web server at EMBL-EBI.[33] Either valine was replaced by phenylalanine at 279, or glutamine was replaced by arginine at 281, or both the residues were changed on the human pPAF-AH sequence to generate sequences with single mutations named as pPAF-AH-V279F or pPAF-AH-Q281R, and double mutation (pPAF-AH-DM) bearing mutations V279F and Q281R.

Model Building and Validation of Wild and Mutant pPAF-AH Enzymes

The 3D X-ray crystal structure of human pPAF-AH enzyme with 374 residues was retrieved from RCSB with PDB Id: 3D59.[15] The missing residues between positions Phe22 to Gln53 at the N-terminus, and missing residues between position His428 to Asn441 at the C-terminus were modeled at the Phyre2 webserver.[34] The missing atoms for residue positions Lys55, Gln88, Asp89, Asn90, Arg91, Arg92, His114, Trp115 and Leu116, were modeled, optimized and minimized on

Discovery Studio 3.5 (Biovia, San Diego, CA). The model was evaluated for stereo chemical and structural correctness using Ramachandran plot, VERIFY3D and ERRAT scores.[35–37] This validated structure was used as a template to model the mutant enzymes pPAF-AH-V279F, pPAF-AH-Q281R and pPAF-AH-DM using SWISS-MODEL.[38] The mutant models were validated for stereo chemical and structural correctness as done for the wild type variant.

Molecular Dynamics Simulations of the Wild and Mutant pPAF-AH Enzymes

The protein models of pPAF-AH, pPAF-AH-V279F, pPAF-AH-Q281R and pPAF-AH-DM were subjected to energy minimization using Gromacs-5 with the AMBER99SB-ILDN force field.[39,40] The models were solvated with a SPC/E water model in a cubic periodic box with 1 nm distance from the edge of the protein atoms. The solvated system was neutralized by two sodium ions. The system was thereafter minimized using the steepest descent algorithm, with convergence criteria of tolerance value of 1000 kJ mol^{-1} nm^{-2}. The complete simulation of minimized solvated proteins was performed under periodic boundary conditions with a time step of 2 fs. Particle mesh Ewald (PME) was used for long range electrostatic interactions with an interpolation order of 4 and a Fourier spacing of 0.16. The first phase simulation was conducted under an NVT ensemble for 500 ps by keeping all bonds constrained using the LINCS algorithm for temperature equilibration. The system was heated to 300 K using leap-frog integrator while pressure coupling was set off. A V-rescale thermostat was used to maintain constant temperature for each system, followed by pressure equilibration at 300 K using Parrinello-Rahman pressure coupling algorithm under an isothermal-isobaric ensemble for another 500 ps at 1.0 bar. Isothermal compressibility of the solvent was set to 4.5e-5 bar−1. Further simulation of 150 ns production run was carried out at 300 K and 1 atm pressure for trajectory analysis. The biophysical properties potential energy, RMSD, radius of gyration, solvent accessible surface area and interaction energies were calculated throughout the dynamics. The final models obtained at the end of MD were validated and taken up for further experiments. The model coordinates were visualized and analyzed using PyMol software.[41]

Docking of PAF to Wild and Mutant Enzymes

The 3D coordinates of substrate PAF was retrieved from PubChem database (CID: 108,156), and was solvated and minimized on Discovery Studio-v3.5 (Biovia, San Diego, CA). This was docked to the models pPAF-AH, pPAF-AH-V279F, pPAF-AH-Q281R and pPAF-AH-DM using the SwissDock web-interface.[42] The poses were clustered, and ranked according to the balanced score comprising of electrostatic, van der Waals and hydrophobic interactions. The top pose complex was refined by MD simulation using the same methodology as in modeling, and the final topologies of the complexes generated were analyzed.

Figure 1 Sequence homology studies of human pPAF-AH enzyme. The sequences in order are human (*Homo sapiens*) pPAF-AH, mouse (*Mus musculus*) pPAF-AH, rabbit (*Oryctolagus cuniculus*) pPAF-AH, wild boar (*Sus scrofa*) pPAF-AH, and sheep (*Ovis aries*) pPAF-AH. Signal sequences at the N-terminus are shown in grey. Conserved catalytic serine, histidine and aspartic acid are shown in bold red and cysteines are shown in bold yellow. Residues at the site of mutation are shown in green/cyan, and green/pink. The UNIPROT accession numbers and percentage homology are given at the end of the sequences. The symbol "*" indicates identical residues, ":" indicates conserved substitution and "." indicates semi-conserved substitution.

Results

Sequence Analysis

Human pPAF-AH enzyme is composed of 441 amino acids, with a mature portion preceded by a 21 residue signal peptide with a cleavage site between Pro21 and Phe22. Among the sequences that were compared, human pPAF-AH has the maximum identity with the rabbit sequence and least with the mouse (Figure 1). While major portions of the sequences are aligned, considerable variations are seen at the C-terminal region. pPAF-AH has a total of five cysteines with the first three of them in conserved positions. The classical serine hydrolase motif GXSXG which has the catalytic serine conserved in the stretch from Gly271 to Gly275. The remaining two active site residues aspartate and histidine at positions 296 and 351, respectively, are conserved. The mutations V279F and Q281R are at positions distal to serine hydrolase motif.

Model Building and Validation

The 3D X-ray crystal structure of human pPAF-AH enzyme (PDB Id: 3D59) had certain residues and atoms that were missing due to weak electron density of the residues.[15] These stretches of residues at the two terminals were modeled by ab-initio and missing atoms on certain residues were modeled by topology modification, while the rest was based on its homology to the crystal structure. The overall structure of the model with 420 residues is shown in Figure 2. Ramachandran plot of this wild pPAF-AH model has 99.0% of the residues lying in favored and allowed regions

Figure 2 Ribbon diagram showing the overall structure of wild human pPAF-AH. Structure derived by homology modelling is shown in green, and structure derived from ab-initio is shown in lemon green. The ten helices are indicated as H1-H10; six short helices are indicated SH1-SH6; and, the eleven beta strands are indicated as β1-β11.

Table 1 Validation of pPAF-AH Models

Model	RMSD (3D59) Å	Ramachandran Plot (%)			Verify 3D Score (%)	ERRAT Quality Factor
		Favored	Allowed	Disallowed		
pPAF-AH-Wild	–	93.3	5.7	1.0	83.10	83.90
pPAF-AH-V279F	0.66	93.5	4.8	1.7	84.76	79.81
pPAF-AH-Q281R	0.67	93.1	5.0	1.9	83.10	89.32
pPAF-AH-DM	0.77	93.8	5.0	1.2	82.38	85.85

(Table 1, Supplementary Figure S1). Dihedral angles of the modeled residues were within the allowed conformations of the plot thereby validating the methodology used. Four residues Asn28, His32, Asp94 and Met430 with disallowed dihedrals lie on loop conformations and away from the catalytic site. Ser273, an active site nucleophile, was observed in strained conformation of marginally allowed region of the Ramachandran plot which is unique and consistent with other α/β serine hydrolase enzymes.[43] VERIFY 3D that describes the compatibility of the model with its amino acid sequence based on secondary structural features and properties of the residues is shown to be more than 80.0%. Errat Quality factor that computes the correctness based on non-bonded interactions was found to be acceptable. This structure was used as a template to build mutant models V279F, Q281R and DM, and these models too were validated. The validated models of wild and mutant variants were then taken up for molecular dynamics.

Biophysical Parameters of the Wild and Mutant pPAF-AH Structures

Trajectory analysis of MD simulation indicates that the system quickly reached the target temperature of 300 K and pressure of 1 bar and remained uniform throughout the equilibration stage (Figure 3A–C). It indicates that the solvent and the ions have attained the right orientation around the protein throughout during the period of equilibration. Under an NPT ensemble with constant number of atoms, pressure, and temperature, the system most closely replicates the experimental conditions. Average density during equilibration phase was found to be

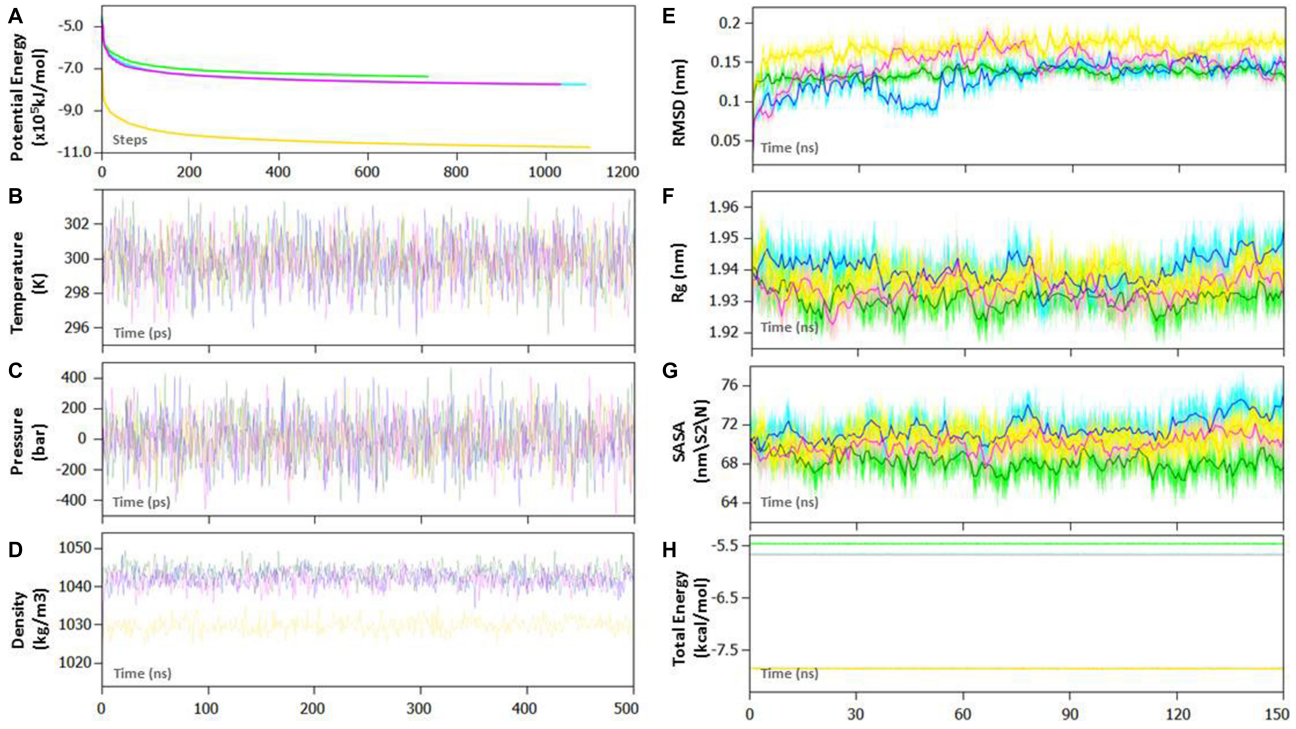

Figure 3 Graphs showing the biophysical parameters for wild pPAF-AH, pPAF-AH-V279F, pPAF-AH-Q281R and pPAF-AH-DM models. Period of equilibration: (**A**) potential energy; (**B**) temperature; (**C**) pressure; (**D**) density, and Molecular dynamics production run: (**E**) rmsd; (**F**) radius of gyration; (**G**) solvent accessible surface area; (**H**) total energy. The plots for wild pPAF-AH, pPAF-AH-V279F, pPAF-AH-Q281R and pPAF-AH-DM are shown in green, cyan, pink and yellow respectively.

Table 2 Biophysical Parameters of Wild and Mutant pPAF-AH Enzymes After Molecular Dynamics Simulation

Biophysical Parameters	Wild	V279F	Q281R	DM
Potential Energy EM (10^5kJ/mol)	−7.09	−7.46	−7.46	−6.43
Potential Energy NVT avg. (10^5kJ/mol)	−6.53	−6.78	−6.79	−5.91
Total Energy NVT avg. (10^5kJ/mol)	−5.41	−5.62	−5.63	−4.89
Potential Energy NPT avg. (10^5kJ/mol)	−6.55	−6.81	−6.82	−5.94
Total Energy NPT avg. (10^5kJ/mol)	−5.43	−5.65	−5.66	−4.92
Density (kg/m^3)	1043.76	1042.18	1041.68	1047.28
Potential Energy MD avg. (10^5kJ/mol)	−6.58	−6.83	−6.83	−5.96
Total Energy MD avg. (10^5kJ/mol)	−5.46	−5.66	−5.67	−4.93
Radius of Gyration backbone (Å)	1.90	2.0	1.98	1.99
Formal charge protein (e)	−2	−2	−1	−1
RMSD_rel_ initial model backbone (Å)	–	1.17	0.90	1.22
Substrate-Binding Area (A^2)	312.9	135.7	49.5	57.1
Substrate-Binding Volume(A^3)	321.2	39.2	12.5	8.3

nearly constant around 1000 kg/m^3 (Figure 3D). The values of potential energy, temperature, pressure and density indicate that the system was stabilized and equipped for the molecular dynamics phase of the experiment (Table 2). The RMSD plot was stable with average deviation of less that 1Å from the mean indicating that the system of protein and solvent has reached a stable state with proteins in optimum conformation (Figure 3E). The radii of gyration and solvent accessible surface area of the three mutant pPAF-AH models are higher than the wild type, less compact and have a higher solvent accessible surface area than its wild type counterpart, suggesting open, less compact and more flexible conformations in the mutants (Figure 3F and G). Total energies were constant for both protein models throughout the course indicating the stability of the systems (Figure 3H). Interestingly, the wild pPAF-AH enzyme model has the highest catalytic binding area and volume suggestive of a possible binding with the substrate (Table 2).

Structural Analysis of the Wild Human pPAF-AH

The overall model of human pPAF-AH crystal structure comprises of 420 amino acids in an α/β-hydrolase fold that has 10 helices, 6 short helices, and 11 β-strands (Figure 2).

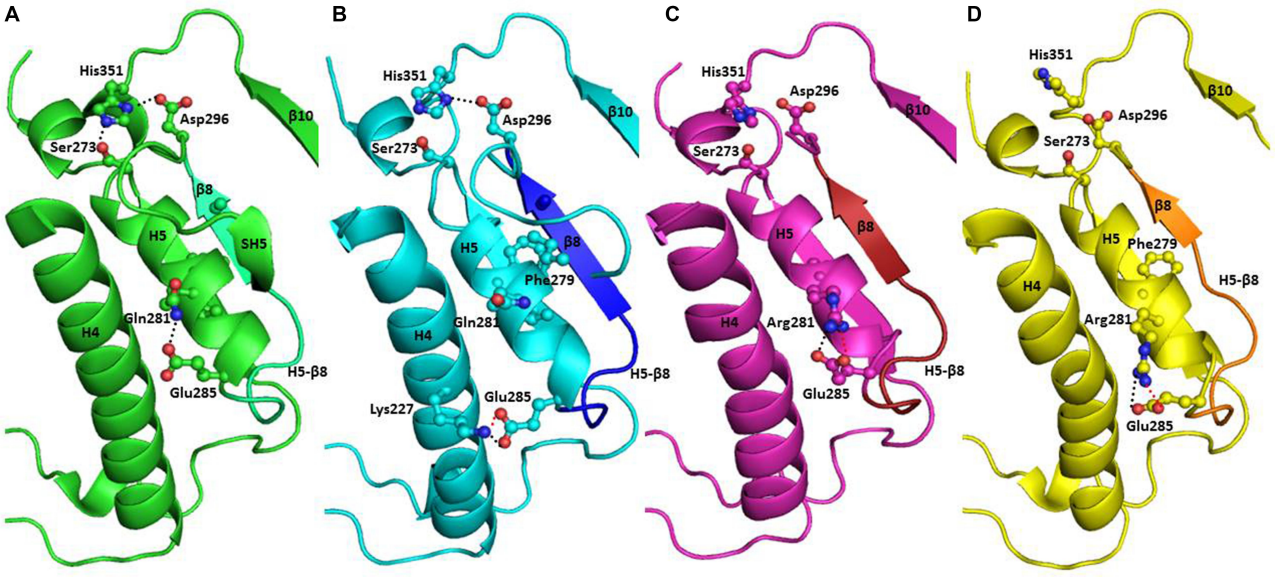

Figure 4 Ribbon diagram showing the site of mutation and catalytic site. (**A**) Wild pPAF-AH (green), (**B**) pPAF-AH-V279F (cyan), (**C**) pPAF-AH-Q281R (pink) and (**D**) pPAF-AH–DM (yellow). Black dotted lines indicate hydrogen bonds, and red dotted bonds indicate ionic bonds. β8 strand is shown in lemon green, dark blue, fire brick and orange in wild pPAF-AH, pPAF-AH-V279F, pPAF-AH-Q281R and pPAF-AH-DM, respectively.

Nine of these β-strands form a part of twisted β-pleated sheets, with the other secondary structures lying on either side of it. The enzyme contains a substrate-binding hydrophobic channel with an active site pocket involving hydrophilic residues interacting to form a catalytic triad.[15] The triad consists of Ser273, Asp296 and His351. Serine 273 lies at the loop connecting β7-H5 helix, Asp296 lies at the loop β8-SH5 and His351 resides on the loop connecting SH6-β10. A 150 ns molecular dynamics simulated trajectory of pPAF-AH shows that Ser273 is consistently making hydrogen bonded interactions with His351 (Ser273 OG … NE2 His351 = 3.1 Å), and His351, in turn, interacts with Asp296 by a hydrogen bond interaction (His351 ND1 … OD2 Asp296 = 2.8 Å) (Figure 4A). The orientation of Asp296 is maintained by two hydrogen bonded interactions with its carboxyl oxygen atoms, one with Ser319 (Asp296 OD2 … OG Ser319 = 2.6 Å), and second with Gln323 (Asp296 OD1 … NE2 Gln323 = 2.8 Å). The orientation of these residues is crucial for activation of nucleophile Ser273 for enzymatic catalysis. The interactions described are consistently present throughout the molecular dynamic simulations.

Site of the Mutation

Mutations at positions 279 and 281 are opposite one another in the middle of the 13 residue long H5 helix (274 to 286) that forms the hydrophobic core of the enzyme (Figure 5). H5 helix lies wedged between H4, the longest helix, and β-sheets β7, β8 and β9. While Val279, at the middle of H5, is surrounded and makes hydrophobic interactions with Val269 on

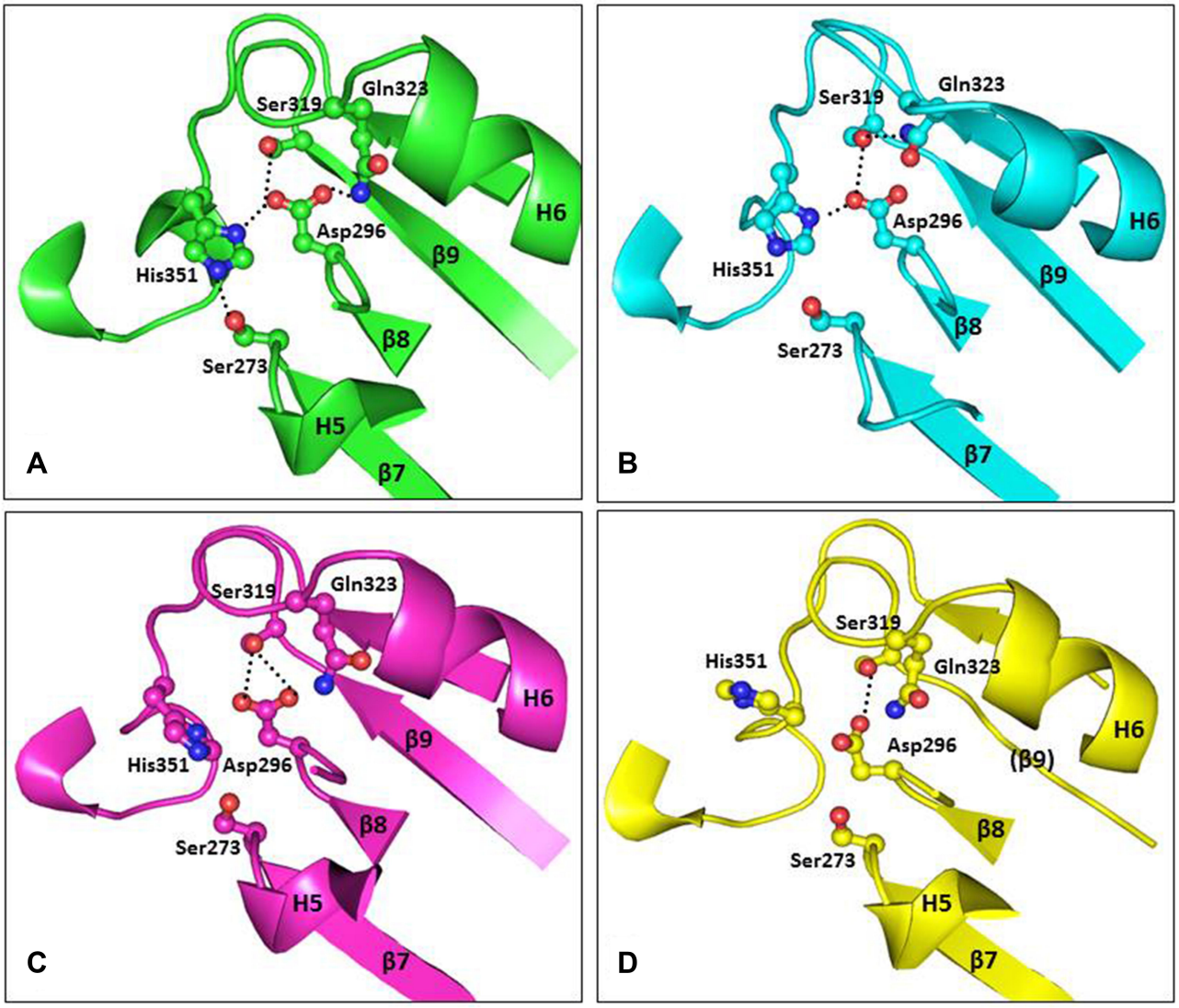

Figure 5 Ribbon diagrams showing catalytic site. (**A**) Wild pPAF-AH (green) Catalytic triad involving hydrogen bonded interactions between active site residues Ser273, His351 and Asp296; (**B**) pPAF-AH-V279F (cyan), (**C**) pPAF-AH-Q281R (pink) and (**D**) pPAF-AH–DM (yellow). Black dotted lines indicate hydrogen bonds.

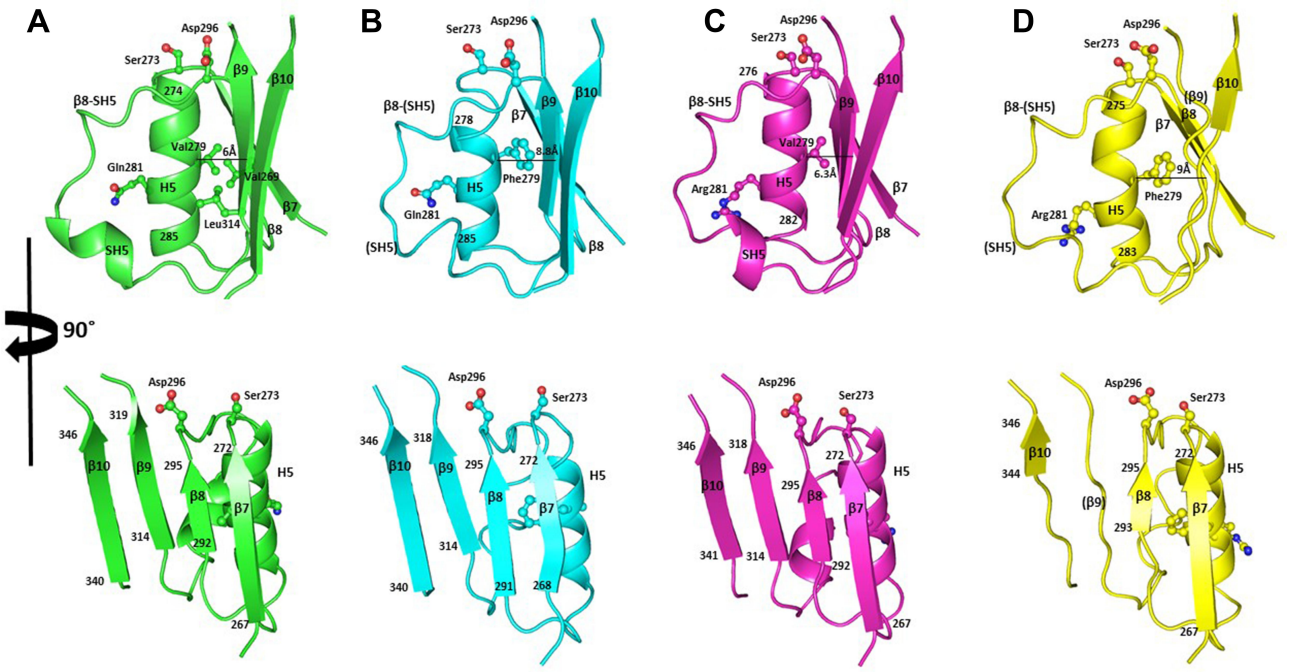

Figure 6 Ribbon diagram showing mutation bearing helix and β-sheets adjacent to it. (**A**) Wild pPAF-AH (green), (**B**) pPAF-AH-V279F (cyan), (**C**) pPAF-AH-Q281R (pink) and, (**D**) pPAF-AH-DM (yellow). Upper panel shows the distance between helix and β-sheet. The hydrophobic interactions of Val279 with Val269 and Leu314 are seen in the wild type, the increase in the distance between H5 and β9 is seen in the mutants bearing Phe279. Lower panel shows the conformations of the secondary structural elements adjacent to it. The lengths of the β-strands β7, β8, β9, and β10 in the wild type and their conversion to loop conformations in the mutants are represented.

β7, and Leu314 on β9 (Figure 6A), Gln281 that lies facing the H4 helix makes a hydrogen bonded interaction with Glu285 (Gln281 NE2 … OE2 Glu285) which lies at the end of the helix (Figure 4A). A loop connects H4 to β8. The main chain subsequent to this forms a loop that has catalytic residue Asp296. Catalytic Ser273 lies on the loop preceding the N-terminal end of H5. It can therefore be inferred that the residue positions 279 and 281 are important in maintaining the conformation and stabilizing the secondary structural elements of the active site for optimum enzymatic function.

Effect of Mutations on the pPAF-AH Conformations

Replacement of valine to a bulky phenylalanine at position 279 on the enzyme (pPAF-AH-V279F) causes a tilt

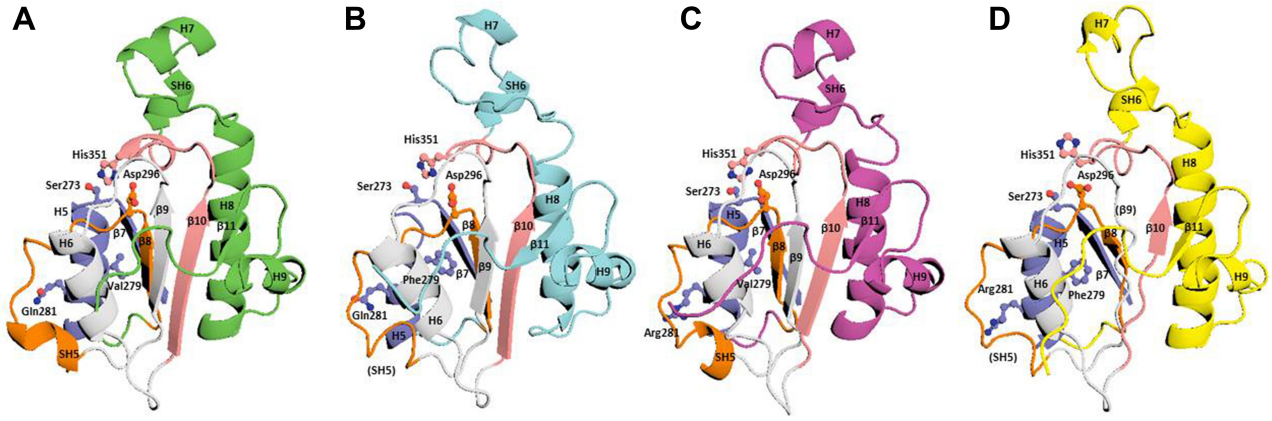

Figure 7 Ribbon diagram showing the secondary structural elements around mutation bearing helix. (**A**) Wild pPAF-AH, (**B**) pPAF-AH-V279F, (**C**) pPAF-AH-Q281R and, (**D**) pPAF-AH-DM. Mutation bearing helix (H5) is shown in purple; Helix H6 is shown in white; beta sheets β7, β8, β9, and β10 are shown in purple, orange, white, and salmon respectively.

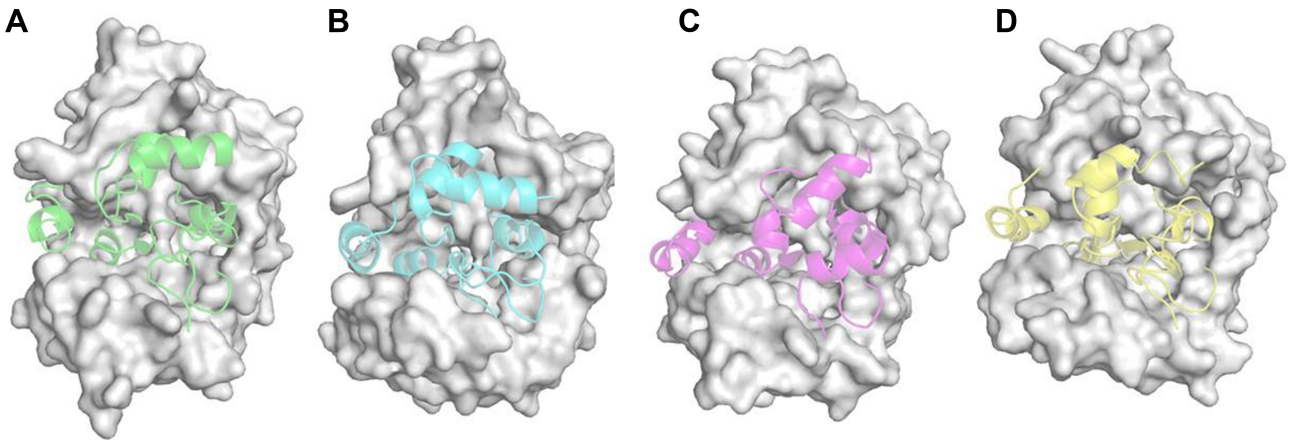

Figure 8 Substrate-binding channel in the wild and mutant pPAF-AH enzymes. Secondary structures of (**A**) wild pPAF-AH (green); (**B**) pPAF-AH-V279F (cyan), (**C**) pPAF-AH-Q281R (pink), and (**D**) pPAF-AH-DM (yellow) that form the substrate-binding hydrophobic channel. Rest of the protein is shown as white GRASP representations. The substrate-binding volume is 321.1 $Å^3$ in the wild type, it is compromised in the mutants (8.3 $Å^3$–39.2 $Å^3$).

in the axis of H5 to avoid steric clashes with the hydrophobic residues on the β-sheets adjacent to it. This change induces subtle conformational changes in the H5-β8 loop, β8 sheet, and the loop bearing Asp296. Glu285 now comes within interacting distance of Lys227 on H4 to form an ionic bonded interaction (Glu285 OE2 … NH Lys227 = 2.5 Å) (Figure 4B). In addition, there is a conformational change of the H6-β9 loop that orients Gln323 away from Asn296, and towards Ser319 which is on the same loop facilitating a hydrogen bonded interaction (Asn296 NE2 … OG Ser319 = 2.5 Å). This results in the shift of His351, which continues to maintain the hydrogen bonded interaction with Asn296 (His351 ND1 … OD2 Asn296 = 2.8 Å). This cascade of interactions induces a change in the orientation of His351 resulting in the loss of hydrogen bonded interaction with catalytic Ser273, rendering pPAF-AH-V279F as a non-functional enzyme (Figure 5B).

Replacement of glutamine to basic arginine on the enzyme pPAF-AH-Q281R causes a shortening of H5 and β8, which induces conformational changes of the loops bearing Ser273 and Asp296, respectively. Glu285 is now on a loop conformation and the flexibility conferred aids in bringing its side chain close to mutational residue Arg281 effecting two interactions, ionic interaction (Glu285 0E2 … NH1 Arg281) and hydrogen bonded interaction (Glu285 OE1 … NH2 Arg281 = 3.4 Å) (Figure 4C. These factors result in change in the orientation of the residues Ser273 and Asp296, thereby causing loss of their interactions with His351 and in turn breaking the catalytic triad, making pPAF-AH-Q281R enzyme non-functional (Figure 5C).

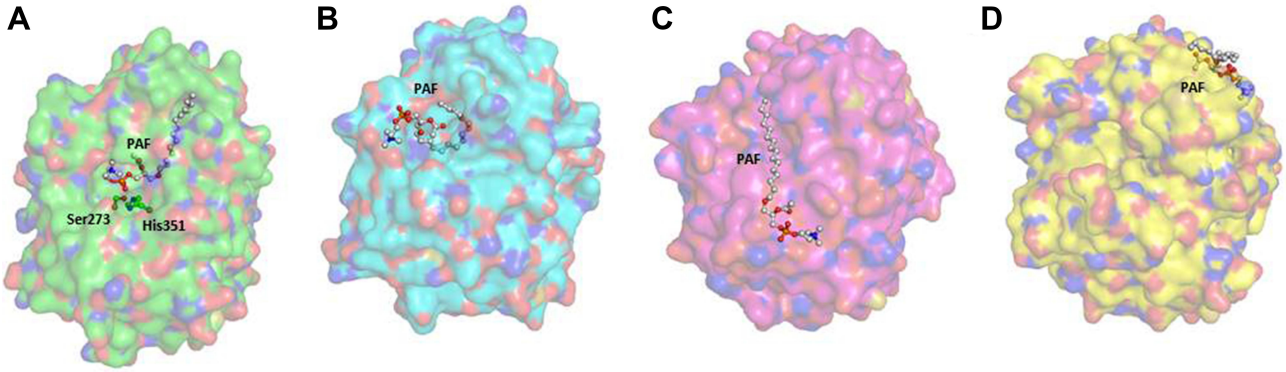

Figure 9 Enzyme-substrate complex. Enzymes are shown in GRASP representation, and the substrate PAF is represented as ball and stick. (**A**) Wild pPAF-AH: PAF complex that shows the enzyme with head of the substrate lying adjacent to the active site residues Ser273 and His351, and the tails occupying the hydrophobic channel. (**B**) pPAF-AH -V279F: PAF complex; (**C**) pPAF-AH-Q281R: PAF complex, and (**D**) pPAF-AH-DM: PAF complex. Substrate PAF does not occupy the hydrophobic channel in the three mutant enzymes.

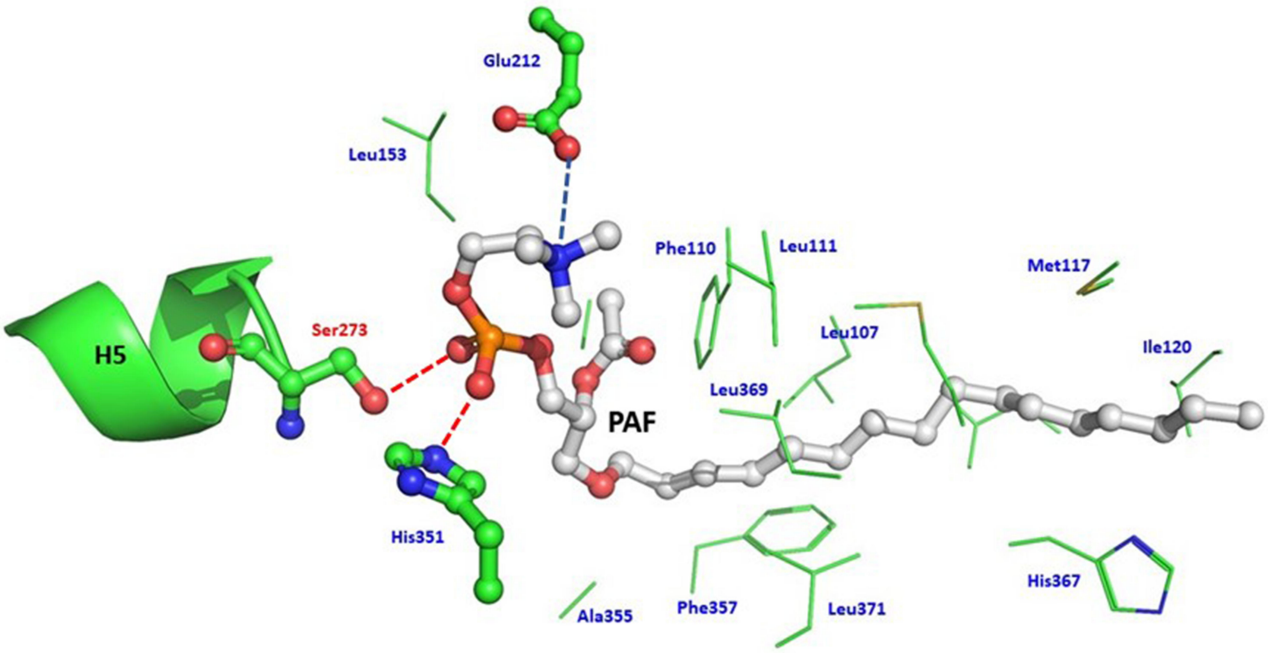

Figure 10 Diagram showing interactions wild type pPAF-AH enzyme with PAF substrate. Catalytic residue Ser273 is shown in ball and stick and labeled in bold red; other residues of the enzyme are shown as lines and labeled in blue; and substrate PAF is shown in ball and stick representation and labeled in bold black. Hydrogen bonded interactions are shown as red dash lines, and salt bridge interactions are shown as blue dash line.

Mutations V279F and Q281R on the enzyme pPAF-AH-DM have a compounding effect on its structural conformations. The presence of bulky Phe279, and basic residue Arg281 induce a further shortening of β8 (Ile293-Leu295) and lengthening of the H5-β8 loop (Ser284-Gly292) (Figure 4D). The change in axis of β8 along with conformational change of β8-SH5 causes a shift of the Asp296 side chain towards His351. His351 therefore flips to the opposite direction to avoid a steric clash, breaking the hydrogen bonded interactions between the catalytic residues, rendering the enzyme pPAF-AH-DM non-functional (Figure 5D).

While the mutation bearing helix H5 is relatively maintained across the wild and mutant structures, there are considerable changes in secondary structural elements around this helix, that bear the three catalytic residues Ser273, Asp296 and His351. Noteworthy among these are: (1) shortening of sheets β7, β8, β9; (2) conversion of SH5 to a loop conformation; (3) conversion of β9 to a loop conformation (Figure 7). These changes account for the increase in the distance between the axis of H5 and plane of β-sheets adjacent to it. This is evident from the increase in the distance between Cα-atom of residue 279 on H5 and Cα-atom of residue 292 on β7 that is 6 Å in the wild type to 9 Å in the double mutant (Figure 6).

Substrate Binding

The conformational changes observed at the site of the mutations and secondary structural elements cause a fivefold decrease in substrate-binding area and a tenfold decrease in substrate-binding volume in the mutant pPAF-AHs (Table 2, Figure 8). Analysis of pPAF-AH:PAF complex shows that the PAF substrate occupies the substrate-binding channel, with the lipid head at the catalytic site and its long hydrophobic chains lying along the length of the channel (Figure 9A). The sessile *sn-2* bond between carbon and oxygen atoms of PAF lies in close proximity to His351 and Ser273 (Ser273 OG ... O5 PAF = 3 Å) (Figure 10). Hydrophobic moieties of the residues in the substrate-binding channel make an array of hydrophobic interactions with the tail of PAF. These interactions are consistent throughout the period of molecular dynamics simulation which reflects their presence and quality (Table 3). However, PAF neither occupies the substrate channel, nor does the sessile bond interact with catalytic residues of the mutant enzymes (Figure 9B–D). It is also evident from molecular dynamics studies that the wild

Table 3 Molecu lar Dynamics Simulation Results of Docked Complex of Wild and Mutant Enzymes with Substrate

Time (ns)	Wild		V279F		Q281R		Double Mutant	
	Electrostatic Interaction Energy (kcal/mol)	Interacting Residues	Electrostatic Interaction Energy (kcal/mol)	Interacting Residues	Electrostatic Interaction Energy (kcal/mol)	Interacting Residues	Electrostatic Interaction Energy (kcal/mol)	Interacting Residues
0	−603.273	L107, F110, L111, M117, L121, L153, G154, S273,W298, H351, Q352, F357, I365, L369	−309.266	Nil	−320.33	L369, K370	−343.554	D250
20	−598.956	L107, L111, G112, G152, L153, A155, Y160, F110, L153, L159, L206, H272, S273,F274,W298, Q352, H351, F357, G366, H367, L369, L371	−422.895	F110, L111, G112, L153, G154, L206, T208, L209, Q352, K370, L371	−567.258	W105, K109, F110, L153, R182, Y205, L206, T208, E214, Y321, F322, Q323, Y324, H351	−446.374	R92, D94, T95, L96, I98, R122, L123, L124, G126, M128, T129, W134,
40	−743.093	L107, F110, L111, M117, I120, L121, F125, G152, L153, A155, Y160, T208, E212, H272, S273, F274, W298, H351, Q352, F354, A355, I364, H367, M368,	−460.651	L209, R207	−499.395	K109, F110, G112, L153, R207, T208, L209, K210, W321, Q323, P325, H351, K370	−541.718	R82, D94, T95, L96, N119, R122, L123, G126, M128, T129, W134, E197, I198, G199, D250
60	−647.918	F110, L111, M117, I120, L121, L124, G152, L153, L159, Y160, E212, H216, H272, S273, H351, Q352, F357, I365, G366, H367, L369	−525.506	F110,L111, G112, L116, I120, L153, L209, K210, E214, R218, F322, Q352, M368,L369, K370	−366.301	K109, G112, T208, L209, E320, Y321, F322, Y324, P325, H351, N421, I422, N423	−387.926	D94, T95, L96, W97, I98, P99, R122, L123, L124, G126, S127, M128
80	−637.192	L107, S108, F110, L111, M117, L121, L153, A155, Y160, T208, E212, H272, S273, F274, W298, H351, Q352, I365, G366, H367, L369, L371	−494.492	F110, L111, L153, K210, E214, F322, Q352, M368, L369, K370	−461.402	K109, F110, L111, G112, L206, R207, T208, E320, Y321, F322, Q323, Y324, H351, N421, I422, N423	−338.013	D94, T95, N100, R122, L123, G126, S127, M128, T129

(*Continued*)

Table 3 (Continued).

Time (ns)	Wild		V279F		Q281R		Double Mutant	
	Electrostatic Interaction Energy (kcal/mol)	Interacting Residues	Electrostatic Interaction Energy (kcal/mol)	Interacting Residues	Electrostatic Interaction Energy (kcal/mol)	Interacting Residues	Electrostatic Interaction Energy (kcal/mol)	Interacting Residues
100	−706.372	L107, S108, F110, L111, M117, I120, L121, G152, G154, A155, Y160, E212, H272, S273, H351, Q352, A355, F357, M368, H367, L369, L371	−384.137	Nil	−409.05	K109, F110, L206, E320, Y321,F322, Q323, Y324, P325, N421, I422, N423	−336.692	D94, P99, I120, R122, L123, G126, S127, M128
120	−635.807	L107, F110, M117, L121, G152, L153, A155, E212, H272, S273, H351, A355, F357, I365, L371	−612.849	L107, F110, L111, M117, L153,G154, L159, T208, L209,E214, R218, Q352, F357, L369, M368, K370	−402.864	G112, R218, S273, F274, W298, E320, Y321, F322, Y324	−340.672	D94, T95, L96, I120, R122,L123, L124, G126, S127, M128, T129
140	−667.714	F110, L111, M117, I120, L121, L124, G152, L153, A155, L159, L206, T208, E212, H216, H272, S273, F274, H351, Q352, F357, T358, T361, H367, M368, L371	−552.962	L59, L107, F110, L111, A155, L209, K210, Q211, E214, S273, F322, H351, Q352, H367, M368, K370, L371	−475.434	F110, L153, L206, T208, R218, F274, A277, W298, M299, F300, P301, L302, Y321, F322, Y324,H351, K370, N423, T424, T425	−397.251	D94, T95, L96, P99, I120, R122, L123, L124, G126, S127, M128, T129,
150	−618.277	L107, F110, M117, L121,G152, L153, A155, E212, H272, S273, H351, A355, F357, I365, L371	−632.945	F110, L111, L121, L159, K210, E214, R218, W298, F322, H351, Q352, F357, M368, L371	−441.782	K109, F110, L111, G112, L206, F274, W298, Y321, F322, Q323, Y324, P325, V350, H351, N423, T424, T425	−348.821	D94, L96, P99, I120, R122, L123, G126, S127, M128, I364

Notes: Catalytic residues having hydrogen bonded interactions are shown in bold red; residues having hydrogen bonded interactions are shown in red; residues having salt bridges are shown in blue; residues having hydrophobic and van der Waals interactions are shown in black.

pPAF-AH-substrate complex is the most stable structure with the optimum number of interactions between them (Supplementary Figure S2). The difference in the enzyme-substrate interactions between the wild and mutant pPAF-AH enzymes can be attributed to channel volume. This parameter could also be a factor responsible for the loss of enzymatic function in the three mutant enzymes, resulting in cardiovascular disease in patients harboring the mutations.[44–46] These structural features delineated in this study therefore place previous

Table 4 Overview of the Function, Structure and Clinical Phenotype of pPAF-AH Mutations

Mutation	Function	Clinical Phenotype	References	Structure	Reference
pPAF-AH-V279F	Activity was 50% lower in heterozygotes; No enzymatic activity in homozygote	Coronary Artery Disease	[44, 47, 48]	• Tilt in the axis of H5 to avoid stearic clashes with the hydrophobic residues on the β-sheets adjacent to it • Conformational changes in the H5-β8 loop, β8 sheet, and the loop bearing Asp296 • Change in the orientation of His351 resulting in loss of hydrogen bonded interaction between His351 and Ser273 • Decrease in substrate-binding area and substrate-binding volume • PAF neither occupies the substrate channel, nor does the sessile bond interact with catalytic residues of the enzyme	This study
pPAF-AH-Q281R	Complete loss of enzyme activity	Coronary Artery Disease	[45]	• Shortening of H5 and β8, induces conformational changes on the loops bearing Ser273 and Asp296, respectively • Glu285 … Arg281 • Change in the orientation of the residues Ser273 and Asp296, resulting in the loss of their interactions with His351 and in turn a loss of the catalytic triad • Decrease in substrate binding area and substrate binding volume • PAF neither occupies the substrate channel, nor does the sessile bond interact with catalytic residues of the enzyme	This study
pPAF-AH-DM	Activity was 50% lower in heterozygotes; No enzymatic activity in homozygote	Coronary Artery Disease	[19]	• Shortening of β8 (Ile293-Leu295) and lengthening of the H5-β8 loop (Ser284-Gly292) • The change in axis of β8 along with conformational change of β8-SH5 causes a shift of Asp296 side chain towards His351 • His 351 therefore flips to the opposite direction breaking the hydrogen bonded interactions between the catalytic residues • Decrease in substrate-binding area and substrate-binding volume • PAF neither occupies the substrate channel, nor does the sessile bond interact with catalytic residues of the enzyme	This study

enzyme assays and clinical studies in the right perspective (Table 4).

Conclusion

As compared to wild type, the mutant pPAF-AH enzymes show changes at the site of the mutation, secondary motif conformations and global structural conformations that affect the orientation of catalytic residues at the active site, a decrease in the substrate channel volume, decrease in stability and structural parameters that are essential for enzymatic function. This study therefore corroborates the previous functional assays and clinical studies, and places the observations in the right perspective. This study also lays the platform to understand the functional and clinical outcomes in pPAF-AH enzymes and provides an opportunity to develop therapeutic interventions to overcome it.

Disclosure

The authors report no conflicts of interest for this work.

References

1. Murakami M, Yoshihara K, Shimbara S, et al. Group IID heparin-binding secretory phospholipase A2 is expressed in human colon carcinoma cells and human mast cells and up-regulated in mouse inflammatory tissues. *Eur J Biochem*. 2002;269(11):2698–2707. doi:10.1046/j.1432-1033.2002.02938.x
2. Van Deenen L, De Haas GH, Heemskerk CT. Hydrolysis of synthetic mixed-acid phosphatides by phospholipase a from human pancreas. *Biochim Biophys Acta*. 1963;67:295–304. doi:10.1016/0926-6569(63)90237-2
3. Valentin E, Lambeau G. Increasing molecular diversity of secreted phospholipases A2 and their receptors and binding proteins. *Biochim Biophys Acta*. 2000;1488(1–2):59–70.
4. Six DA, Dennis EA. The expanding superfamily of phospholipase A2 enzymes: classification and characterization. *Biochim Biophys Acta*. 2000;1488(1–2):1–19.
5. Balsinde J, Winstead MV, Dennis EA. Phospholipase A2 regulation of arachidonic acid mobilization. *FEBS Lett*. 2002;531(1):2–6. doi:10.1016/S0014-5793(02)03413-0

6. Dufton MJ, Hider RC. Classification of phospholipases A2 according to sequence. Evolutionary and pharmacological implications. *Eur J Biochem*. 1983;137(3):545–551. doi:10.1111/j.1432-1033.1983.tb07860.x
7. Schaloske RH, Dennis EA. The phospholipase A2 superfamily and its group numbering system. *Biochim Biophys Acta*. 2006;1761(11):1246–1259.
8. Tarricone C, Perrina F, Monzani S, et al. Coupling PAF signaling to dynein regulation: structure of LIS1 in complex with PAF-acetylhydrolase. *Neuron*. 2004;44(5):809–821.
9. Camejo G. Lysophospholipids: effectors mediating the contribution of dyslipidemia to calcification associated with atherosclerosis. *Atherosclerosis*. 2010;211(1):36–37. doi:10.1016/j.atherosclerosis.2010.02.005
10. Rodriguéz-Lee M, Bondjers G, Camejo G. Fatty acid-induced atherogenic changes in extracellular matrix proteoglycans. *Curr Opin Lipidol*. 2007;18(5):546–553. doi:10.1097/MOL.0b013e3282ef534f
11. Tsimikas S, Mallat Z, Talmud PJ, et al. Oxidation-specific biomarkers, lipoprotein (a), and risk of fatal and nonfatal coronary events. *J Am Coll Cardiol*. 2010;56(12):946–955. doi:10.1016/j.jacc.2010.04.048
12. Adachi H. cDNA cloning and expression of intracellular platelet-activating Factor(PAF) acetylhydrolase II. Its homology with plasma paf acetylhydrolase. *J Biol Chem*. 1996;271:51.
13. Graham RM, Stephens CJ, Silvester W, Leong L, Sturm MJ, Taylor RR. Plasma degradation of platelet-activating factor in severely ill patients with clinical sepsis. *Crit Care Med*. 1994;22(2):204–212. doi:10.1097/00003246-199402000-00009
14. Tjoelker LW, Wilder C, Eberhardt C, et al. Anti-inflammatory properties of a platelet-activating factor acetylhydrolase. *Nature*. 1995;374(6522):549–553. doi:10.1038/374549a0
15. Samanta U, Bahnson BC. Crystal structure of human plasma platelet-activating factor acetylhydrolase structural implication to lipoprotein binding and catalysis. *J Biol Chem*. 2008;283(46):31617–31624. doi:10.1074/jbc.M804750200
16. Xu H, Iijima K, Shirakawa T, et al. Platelet-activating factor acetylhydrolase gene mutation in Japanese children with Escherichia coli O157–associated hemolytic uremic syndrome. *Am J Kidney Dis*. 2000;36(1):42–46. doi:10.1053/ajkd.2000.8262
17. Yamada Y, Ichihara S, Fujimura T, Yokota M. Identification of the G994→ T missense mutation in exon 9 of the plasma platelet-activating factor acetylhydrolase gene as an independent risk factor for coronary artery disease in Japanese men. *Metabolism*. 1998;47(2):177–181. doi:10.1016/S0026-0495(98)90216-5
18. Dennis EA, Cao J, Hsu Y-H, Magrioti V, Kokotos G. Phospholipase A2 enzymes: physical structure, biological function, disease implication, chemical inhibition, and therapeutic intervention. *Chem Rev*. 2011;111(10):6130–6185. doi:10.1021/cr200085w
19. Stafforini DM, Satoh K, Atkinson DL, et al. Platelet-activating factor acetylhydrolase deficiency. A missense mutation near the active site of an anti-inflammatory phospholipase. *J Clin Invest*. 1996;97(12):2784–2791.
20. Kruse S, Mao X-Q, Heinzmann A, et al. The Ile198Thr and Ala379Val variants of plasmatic PAF-acetylhydrolase impair catalytical activities and are associated with atopy and asthma. *Am J Hum Genet*. 2000;66(5):1522–1530. doi:10.1086/302901
21. Lavi S, Herrmann J, Lavi R, McConnell JP, Lerman LO, Lerman A. Role of lipoprotein-associated phospholipase A2 in atherosclerosis. *Curr Atheroscler Rep*. 2008;10(3):230. doi:10.1007/s11883-008-0036-9
22. Ishihara M, Iwasaki T, Nagano M, et al. Functional impairment of two novel mutations detected in lipoprotein-associated phospholipase A2 (Lp-PLA2) deficiency patients. *J Hum Genet*. 2004;49(6):302–307. doi:10.1007/s10038-004-0151-6
23. Jang Y, Kim OY, Koh SJ, et al. The Val279Phe variant of the lipoprotein-associated phospholipase A2 gene is associated with catalytic activities and cardiovascular disease in Korean men. *J Clin Endocrinol Metab*. 2006;91(9):3521–3527. doi:10.1210/jc.2006-0116
24. Min J-H, Wilder C, Aoki J, et al. Platelet-activating factor acetylhydrolases: broad substrate specificity and lipoprotein binding does not modulate the catalytic properties of the plasma enzyme. *Biochemistry*. 2001;40(15):4539–4549. doi:10.1021/bi002600g
25. Khan MI, Hariprasad G. Human secretary phospholipase A2 mutations and their clinical implications. *J Inflamm Res*. 2020;13:551–561. doi:10.2147/JIR.S269557
26. Hariprasad G, Hariprasad G, Singh B, et al. Cloning, sequence analysis and homology modeling of a novel phospholipase A2 from heterometrusfulvipes (Indian black scorpion) full length research paper. *DNA Seq*. 2007;18(3):242–246.
27. Hariprasad G, Srinivasan A, Singh R. Structural and phylogenetic basis for the classification of group III phospholipase A2. *J Mol Model*. 2013;19(9):3779–3791. doi:10.1007/s00894-013-1913-x
28. Hariprasad G, Kaur P, Srinivasan A, Singh TP, Kumar M. Structural analysis of secretory phospholipase A2 from clonorchis sinensis: therapeutic implications for hepatic fibrosis. *J Mol Model*. 2012;18(7):3139–3145. doi:10.1007/s00894-011-1333-8
29. Hariprasad G, Kumar M, Kaur P, Singh TP, Kumar RP. Human group III PLA2 as a drug target: structural analysis and inhibitor binding studies. *Int J Biol Macromol*. 2010;47(4):496–501. doi:10.1016/j.ijbiomac.2010.07.004
30. Hariprasad G, Kota D, Singh SB, Srinivasan A, Adhikary S. Delineation of the structural elements of oriental liver fluke PLA 2 isoforms for potent drug designing. *Indian J Clin Biochem*. 2014;29(4):430–441. doi:10.1007/s12291-013-0377-1
31. Khan MI, Gupta AK, Kumar DR, Kumar M, Ethayathulla AS, Hariprasad G. Molecular modeling of Gly80 and Ser80 variants of human group IID phospholipase A2 and their receptor complexes: potential basis for weight loss in chronic obstructive pulmonary disease. *J Mol Model*. 2016;22(9):232.
32. Coordinators NR. Database resources of the national center for biotechnology information. *Nucleic Acids Res*. 2015;43(D1):D6–D17.
33. Madeira F, Park YM, Lee J, et al. The EMBL-EBI search and sequence analysis tools APIs in 2019. *Nucleic Acids Res*. 2019;47(W1):W636–W641. doi:10.1093/nar/gkz268
34. Kelley LA, Mezulis S, Yates CM, Wass MN, Sternberg MJE. The Phyre2 web portal for protein modeling, prediction and analysis. *Nat Protoc*. 2015;10(6):845–858. doi:10.1038/nprot.2015.053
35. Ramachandran GN, Ramakrishnan C, Sasisekharan V. Stereochemistry of polypeptide chain configurations. *J Mol Biol*. 1963;7(1):95–99. doi:10.1016/S0022-2836(63)80023-6
36. Eisenberg D, Lüthy R, Bowie JU. VERIFY3D: assessment of protein models with three-dimensional profiles. In: *Methods in Enzymology*. Vol. 277. Elsevier; 1997:396–404.
37. Colovos C, Yeates T. ERRAT: an empirical atom-based method for validating protein structures. *Protein Sci*. 1993;2(9):1511–1519. doi:10.1002/pro.5560020916
38. Waterhouse A, Bertoni M, Bienert S, et al. SWISS-MODEL: homology modelling of protein structures and complexes. *Nucleic Acids Res*. 2018;46(W1):W296–W303. doi:10.1093/nar/gky427
39. Lindorff-Larsen K, Maragakis P, Piana S, Eastwood MP, Dror RO, Shaw DE. Systematic validation of protein force fields against experimental data. *PLoS One*. 2012;7(2):e32131. doi:10.1371/journal.pone.0032131
40. Beauchamp KA, Lin Y-S, Das R, Pande VS. Are protein force fields getting better? A systematic benchmark on 524 diverse NMR measurements. *J Chem Theory Comput*. 2012;8(4):1409–1414. doi:10.1021/ct2007814
41. Schrodinger L. *The PyMol Molecular Graphics System, Version 2.0*. New York, NY: Schrödinger, LLC; 2017.
42. Grosdidier A, Zoete V, Michielin O. SwissDock, a protein-small molecule docking web service based on EADock DSS. *Nucleic Acids Res*. 2011;39(suppl_2):W270–W277.
43. Ollis DL, Cheah E, Cygler M, et al. The α/β hydrolase fold. *Protein Eng Des Sel*. 1992;5(3):197–211. doi:10.1093/protein/5.3.197

44. Unno N, Nakamura T, Kaneko H, et al. Plasma platelet-activating factor acetylhydrolase deficiency is associated with atherosclerotic occlusive disease in Japan. *J Vasc Surg*. 2000;32(2):263–267. doi:10.1067/mva.2000.105670
45. Yamada Y, Yokota M. Loss of activity of plasma platelet-activating factor acetylhydrolase due to a novel Gln281→ Arg mutation. *Biochem Biophys Res Commun*. 1997;236(3):772–775. doi:10.1006/bbrc.1997.7047
46. Stafforini DM, Numao T, Tsodikov A, et al. Deficiency of platelet-activating factor acetylhydrolase is a severity factor for asthma. *J Clin Invest*. 1999;103(7):989–997. doi:10.1172/JCI5574
47. Widodo W, Ramadhani AN, Nofitasari A, et al. The V279F polymorphism might change protein character and immunogenicity in Lp-PLA2 protein. *Egypt J Med Hum Genet*. 2018;19(2):107–112. doi:10.1016/j.ejmhg.2017.08.001
48. Li L, Qi L, Lv N, et al. Association between lipoprotein-associated phospholipase A2 gene polymorphism and coronary artery disease in the Chinese Han population. *Ann Hum Genet*. 2011;75(5):605–611. doi:10.1111/j.1469-1809.2011.00666.x